

Nature of the spin-glass phase in dense packings of Ising dipoles with random anisotropy axes

Juan J. Alonso^{1,2,*} and B. Allés^{3,†}

¹*Física Aplicada I, Universidad de Málaga, 29071 Málaga, Spain*

²*Instituto Carlos I de Física Teórica y Computacional, Universidad de Granada, 18071 Granada, Spain*

³*INFN-Sezione di Pisa, Largo Pontecorvo 3, 56127 Pisa, Italy*

(Dated: August 19, 2021)

Using tempered Monte Carlo simulations, we study the spin-glass phase of dense packings of Ising dipoles pointing along random axes. We consider systems of L^3 dipoles (a) placed on the sites of a simple cubic lattice with lattice constant d , (b) placed at the center of randomly closed packed spheres of diameter d that occupy a 64% of the volume. For both cases we find an equilibrium spin-glass phase below a temperature T_{sg} . We compute the spin-glass overlap parameter q and their associated correlation length ξ_L . From the variation of ξ_L with T and L we determine T_{sg} for both systems. In the spin-glass phase, we find (a) $\langle q^2 \rangle$ decreases algebraically with L , and (b) ξ_L/L does not diverge as L increases. At very low temperatures we find comb-like distributions of q that are sample-dependent. We find that the fraction of samples with cross-overlap spikes higher than a certain value as well as the average width of the spikes are size independent quantities. All these results are consistent with a quasi-long-range order in the spin-glass phase, as found previously for very diluted dipolar systems.

PACS numbers: 75.10.Nr, 75.10.Hk, 75.40.Cx, 75.50.Lk

I. INTRODUCTION

The collective behavior of systems of interacting dipoles (SID) has received renewed attention in the last few years.¹ This is due to the fact that recent advances in nanoscience² allow to create new magnetic materials made of ensembles of identical interacting nanoparticles (NP),^{3,4} in contrast with conventional magnets. Materials built with ensembles of NP are of interest for data storage⁵ and have applications in biomedicine.⁶

Ferromagnetic NP with sizes up to a few tens of nanometers include a single magnetic domain. This domain behaves as a dipole with magnetic moment ranging from 10^2 to $10^4 \mu_B$ (μ_B is the Bohr magneton). NP exhibit effective anisotropies as a consequence of either magnetocrystalline or shape or surface effects. These anisotropies provoke the appearance of one or more easy axes in each NP, along one of which the related dipole tends to align. Thus, the dipole is forced to overcome a certain energy barrier E_a during any possible flipping process between the two directions of magnetization along one of the easy axes.

When NP ensembles are packed in frozen arrays of well separated (not touching) particles, the dipolar becomes the only relevant particle-particle interaction among individual NP. Moreover, for sufficiently concentrated ensembles, dipolar interparticle energies E_{dd} may be comparable or even larger than the local E_a . In such cases, cooperative behavior among dipoles could be observed at low temperatures⁴ (instead of the super-paramagnetism observed in weakly interacting systems with $E_{dd} \ll E_a$).⁷

The anisotropy of the dipolar interaction leads to geometric *frustration*⁸ when dipoles are placed in crystalline arrays. This results in collinear antiferromagnetic (ferromagnetic) order in simple cubic lattices (face and body

centered lattices) as predicted time ago by Luttinger and Tisza,⁹ and observed recently in crystals build with NP.^{10,11}

Disordered (non-crystalline) dense arrays of NP can be obtained from colloidal dispersions of particles in frozen fluids,¹² or by compacting powders of NP in granular solids.^{4,13} The typical volume fractions attained by those systems range from 20 to 40%. As pointed out by Mørup,¹⁴ frozen *disorder* in the position of each NP and/or in its random orientation together with *frustration* (that comes from dipolar interactions) may result in spin-glass (SG) behavior.^{8,15} These systems are often called *super-SGs*, because they are made of NP. They exhibit typical behavior of SG¹⁶ such as anomalous relaxation, aging, and other memory effects similar to the ones previously found in their single-molecule SG counterparts.¹⁷ Numerical simulations of SID with different combinations of positional and easy-axis orientational disorder have revealed a similar behavior,^{18–23} and also that, irrespective of the relative dipolar interaction strength, dipoles flip up or down along their local easy axes in an Ising-like manner.²⁴ SG behavior clearly governed by dipolar interactions has been observed in random closed packed (RCP) samples of highly monodisperse maghemite (γFe_2O_3) NP.^{25,26}

Recent Monte Carlo (MC) simulations of diluted systems of either parallel^{27–29} or randomly oriented Ising dipoles³⁰ exhibited the existence of a SG phase at temperatures below a transition temperature T_{sg} . Moreover, MC data are consistent with quasi-long-range³¹ order in the SG phase.^{28,29} Neither the droplet model³² nor a replica symmetry breaking (RSB) scenario³³ fit in with this marginal behavior. Previous MC work for a fully occupied simple cubic (SC) lattice of dipoles with randomly oriented axes³⁴ also found a SG phase, but nei-

ther clear-cut results about the nature of the SG phase were obtained, nor was it possible to discern between the above mentioned scenarios. The validity of one scenario over the others may depend crucially on the interactions involved in the system under study. A paradigmatic model that exhibits RSB is the Sherrington-Kirkpatrick (SK) model,^{35,36} where the couplings between pairs of spins are chosen randomly to be ferromagnetic or anti-ferromagnetic regardless of the spin-spin distance. However, the applicability of a RSB scenario to more realistic (short-ranged) models as the Edwards-Anderson^{38,39} is still controversial.¹⁵

The main purpose of the present work is to investigate by tempered MC simulations the equilibrium SG phase of dense packings of randomly oriented Ising dipoles. We consider arrays of dipoles placed on the sites of a fully-occupied SC lattice, and ensembles of dipoles placed at the center of RCP spheres that occupy a 64% fraction of the entire volume. Both packings are clearly more homogeneous than loose-packed configurations with lower volume fraction, or diluted fluid-like positional configurations in which the number of neighbors changes greatly from particle to particle.

We measure the overlap parameter q between equilibrium configurations, its associated correlation length, as well as sample-to-sample fluctuations of probability distributions of q for different realizations of disorder.

The paper is organized as follows. In Sec. II we define the model and the types of dense packings we use, give details on the MC algorithm, and define the quantities we compute. The results are presented in Sec. III and some concluding remarks in Sec. IV.

II. MODELS, METHOD, AND MEASURED QUANTITIES

A. Models

We study the low temperature behavior of dense packings of identical magnetic NP that behave as single magnetic dipoles. Each NP i is a hard sphere of diameter d carrying a permanent pointlike magnetic moment $\vec{\mu}_i = \mu\sigma_i\hat{a}_i$ at its center. \hat{a}_i is the local easy-axis and $\sigma_i = \pm 1$ is a sign representing the moment $\vec{\mu}_i$ pointing up or down along \hat{a}_i . $\mu \equiv \|\vec{\mu}_i\|$ is equal for all dipoles. As in real dense packings of NP, we consider that \hat{a}_i axes are frozen and point along randomly distributed directions. Magnetic moments are coupled solely by dipolar interactions. The Hamiltonian is given by

$$\mathcal{H} = \varepsilon_d \sum_{\langle i,j \rangle} \left(\frac{d}{r_{ij}} \right)^3 \left(\hat{a}_i \cdot \hat{a}_j - \frac{3(\hat{a}_i \cdot \vec{r}_{ij})(\hat{a}_j \cdot \vec{r}_{ij})}{r_{ij}^2} \right) \sigma_i \sigma_j \quad (1)$$

where $\varepsilon_d = \mu_0\mu^2/(4\pi d^3)$ is an energy (μ_0 is the magnetic permeability in vacuum), and the summation runs over

all pairs of particles i and j except $i = j$. \mathcal{H} can be recast in the manifestly Ising-like form

$$\mathcal{H} = \sum_{\langle i,j \rangle} T_{ij} \sigma_i \sigma_j \quad (2)$$

where,

$$T_{ij} = \varepsilon_d \left(\frac{d}{r_{ij}} \right)^3 \left(\hat{a}_i \cdot \hat{a}_j - \frac{3(\hat{a}_i \cdot \vec{r}_{ij})(\hat{a}_j \cdot \vec{r}_{ij})}{r_{ij}^2} \right). \quad (3)$$

Since dipoles point along randomly chosen directions \hat{a}_i , T_{ij} signs are distributed at random. Moreover, T_{ij} values depend on the orientation and on the modulus of the relative position vectors \vec{r}_{ij} .

In our simulations we flip dipoles up and down along their easy axes. Given that we are not interested on time dependent properties controlled by the interplay between local anisotropy and interparticle dipolar energies, we do not try to mimic how each dipole overcomes anisotropy barriers. Rather, we try to reproduce the collective evolution effects that follow when the system is allowed to explore the rough free-energy landscape inherent to SG and relax to equilibrium.

We shall analyze two different types of packings of identical spheres. On the one hand, the spheres have been placed on the nodes of SC lattices with lattice spacing d , and on the other hand, they have been placed in random close packings (RCP). Both types of packings are collectively called random axial dipole systems (RAD). We do not expect to see relevant differences in the behavior of the two packings, because both are rather homogeneous and dominated by a random axis distribution.

As for RCP, many experimental results and numerical simulations indicate that in the most compact way, RCP spheres occupy a volume fraction $\phi = \phi_0 \equiv 0.64$.⁴² For that reason, we choose RCP systems with this precise value of ϕ . Note that there is an additional source of randomness in RCP stemming from the spatial disorder in \vec{r}_{ij} .

For comparison, we study also the SK model: a set of N Ising spins $\sigma_i = \pm 1$ where any pair of spins interacts. The interaction energies between the spins at sites i and j is $J_{ij}\sigma_i\sigma_j$ with $J_{ij} = \pm 1/\sqrt{N}$. The signs in J_{ij} are chosen randomly.

In the following, all temperatures will be given in units of ε_d/k_B ($1/k_B$ for the SK model), where k_B is Boltzmann's constant.

B. Method

We have simulated N_s independent *samples* of the above-described models. A *sample* \mathcal{J} is a given realization of quenched disorder. For RAD systems this disorder means choosing the orientations of vectors \hat{a}_i randomly, while a sample for the SK model is defined by the distribution of signs in J_{ij} . Besides the disorder in the

orientations of \hat{a}_i , RCP systems include another source of disorder, namely the positions \vec{r}_i of the spheres. This second cause of disorder is absent in SC systems.

To fix \vec{r}_i in RCP systems, the Lubachevsky-Stillinger (LS) algorithm^{40,41} has been used. With it, a system of N identical hard spheres evolve according to Newtonian dynamics. At the same time, all the particles are let to grow in size. Furthermore, this growth is performed at a sufficiently high rate in order to avoid the system ending up in a crystalline state. Proceeding in this way, at the end the system gets up stuck in a disordered state.^{41,42} To be precise, we start placing a Poisson distribution of N small spheres by random sequential addition in a cube whose edges have length $L = 1$. At the beginning the spheres occupy a volume fraction $\phi = 0.2$. Periodic boundary condition are applied. The LS algorithm lets spheres move freely and grow until the sample eventually reaches the volume fraction ϕ_0 .⁴¹ Finally, once the LS algorithm has stopped evolving the spheres and their size, positions \vec{r}_i are rescaled such that all spheres recover a diameter $d = 1$ and L becomes $L = (N\pi/6\phi_0)^{1/3}$.

The system size is determined by the number N of spheres. The number of samples N_s is listed in Tables I and II for every size N . In SG systems statistical errors are independent of N because of their inherent lack of self-averaging. This is why we have not made N_s smaller with increasing N . For RAD systems in SC lattices with $N = 1000$, we could only employ 1400 samples because of CPU time limitations.

Periodic boundary conditions are always used. We let each dipole i interact with the other dipoles within an $L \times L \times L$ cube centered on i and with the repeated copies of the dipoles beyond the box (by periodicity). In order to take into account the slowly decaying long-range dipole-dipole interaction we do perform Ewalds's summations.^{43,44} We follow the notation from the paper by Wang and Holm.⁴⁵ In this method, pointlike dipoles are screened by Gaussians with standard deviation $1/2\alpha$ that allow to split the computation of the dipolar energy into two rapidly convergent sums, one in real space and the other in reciprocal space. We evaluate the sum in real space using the normal image convention, with a cutoff $r_c = L/2$. Also a reciprocal space cutoff k_c is introduced for the sum in the reciprocal space. We have chosen $k_c = 10$, and $\alpha = 7.9/L$ as a good compromise between accuracy and calculation speed.⁴⁵ Finally, given that our system is expected to exhibit zero magnetization, we have used a surrounding permeability $\mu' = 1$.

In order to reach equilibrium at low temperatures in the SG phase we use a parallel tempered Monte Carlo (TMC) algorithm.⁴⁶ It consists in running a set of n identical replicas of each sample in parallel at different temperatures in the interval $[T_{min}, T_{max}]$ with a separation Δ between neighboring temperatures. Each replica starts from a completely disordered configuration $\{\sigma_i\}$. We apply the TMC algorithm in two steps. In the first one, the n replicas of the sample \mathcal{J} evolve independently for 8 Metropolis sweeps.⁴⁷ All dipolar fields throughout

the system are updated every time a spin flip is accepted. In the second step, we give to any pair of replicas evolving at temperatures T and $T - \Delta$ a chance to exchange states between them following standard tempering rules which satisfy detailed balance.⁴⁶ These exchanges allow all replicas to diffuse back and forth from low to high temperatures and reduce equilibration times for the rough energy landscapes expected for SGs. We find it helpful to choose T_{max} larger than $2 \times T_{sg}$ and choose Δ such that at least 30% of all attempted exchanges are accepted for all pairs $(T, T - \Delta)$.

Measurements were taken after two averagings: firstly over thermalized states of a given sample \mathcal{J} and secondly over N_s samples with different realizations of quenched disorder. Thermal averages come from averaging over the time interval $[t_0, 2t_0]$, where t_0 is the equilibration time. Given an observable \mathbf{u} , $u_{\mathcal{J}} = \langle \mathbf{u} \rangle_T$ stands for the thermal average of sample \mathcal{J} and $\langle u \rangle = [u_{\mathcal{J}}]_{\mathcal{J}}$ for the average over samples. The values of various parameters used in the simulation runs are given in Tables I and II.

Simple Cubic					
N	T_{min}	T_{max}	Δ	t_0	N_s
64	0.2	2.1	0.05	8×10^6	5100
125	0.2	2.1	0.05	8×10^6	10000
216	0.2	2.1	0.05	8×10^6	10000
343	0.2	2.1	0.05	8×10^6	4800
512	0.2	2.1	0.05	8×10^6	5100
1000	0.6	2.1	0.05	10^7	1400
Random Close Packaged					
N	T_{min}	T_{max}	Δ	t_0	N_s
125	0.2	2.1	0.05	8×10^6	5900
216	0.2	2.1	0.05	8×10^6	8000
512	0.2	2.1	0.05	8×10^6	7700

TABLE I. Simulation parameters for SC and RCP systems. N is the number of dipoles, T_{min} (T_{max}) is the lowest (highest) temperature and Δ is the temperature step in our TMC simulations. The number of simulation sweeps for equilibration is t_0 . Measurements are taken in the time interval $[t_0, 2t_0]$. The number of samples with different realizations of quenched disorder is N_s .

N	T_{min}	T_{max}	Δ	t_0	N_s
64	0.16	1.60	0.04	10^5	10^5
216	0.16	1.60	0.04	10^5	1.4×10^5
512	0.16	1.60	0.04	2×10^5	10^5

TABLE II. Same as in Table I for the SK model.

C. Observables

The SG behavior has been investigated by measuring the spin overlap parameter,³⁸

$$q \equiv N^{-1} \sum_j \sigma_j^{(1)} \sigma_j^{(2)}, \quad (4)$$

where $\sigma_j^{(1)}$ and $\sigma_j^{(2)}$ are the spins on site j of two independent equilibrium states, called (1) and (2), of a given sample. Clearly, q is a measure of the spin configuration overlap between the two states. To avoid unwanted correlations, we do not look for states (1) and (2) in single samples. Rather, we consider for each sample, a pair of identical replicas that evolve independently in time.

We evaluate the order parameters $q_2 \equiv \langle q^2 \rangle$ and $q_1 \equiv \langle |q| \rangle$ and, for each sample \mathcal{J} the overlap probability distribution $p_{\mathcal{J}}(q)$. Then, the mean overlap distribution $p(q)$ over all replicas is defined as

$$p(q) \equiv [p_{\mathcal{J}}(q)]_{\mathcal{J}}. \quad (5)$$

We also measure the mean square deviations of $p_{\mathcal{J}}(q)$, from the average $p(q)$,

$$\delta p(q)^2 \equiv [\{ p_{\mathcal{J}}(q) - p(q) \}^2]_{\mathcal{J}}. \quad (6)$$

As usual in SG work,^{48–50} the correlation length ξ_L is computed by

$$\xi_L^2 \equiv \frac{1}{4 \sin^2(k/2)} \left\{ \frac{\langle q^2 \rangle}{\langle |q(\mathbf{k})|^2 \rangle} - 1 \right\}, \quad (7)$$

where

$$q(\mathbf{k}) \equiv N^{-1} \sum_j \psi_j e^{i\vec{k} \cdot \vec{r}_j}, \quad (8)$$

with $\psi_j \equiv \sigma_j^{(1)} \sigma_j^{(2)}$, \vec{r}_j the position of dipole j , and $\vec{k} = (2\pi/L, 0, 0)$ and $k = \|\vec{k}\| = 2\pi/L$. Recall that since our systems are isotropic, all directions \vec{k} are equivalent.

The correlation function $\langle \psi_r \psi_0 \rangle - \langle \psi_r \rangle \langle \psi_0 \rangle$ decays as $\exp(-r/\xi_\infty)$ where ξ_∞ is the correlation length in the thermodynamic limit. ξ_L in (7) provides a good approximation of ξ_∞ in the $\xi_L/L \rightarrow 0$ limit in the paramagnetic phase for which $\langle \psi_r \rangle$ vanishes.⁴⁹

This is not the case for an ordered phase. Consider for example strong long-range order with short-range order fluctuations. That is, $\langle \psi_0 \psi_r \rangle$ does not vanish as $r \rightarrow \infty$ and only $\langle \psi_0 \psi_r \rangle - \langle \psi_0 \rangle \langle \psi_r \rangle$ is short-range. In such a case, the ratio $(\xi_L/L)^2$ diverges as L^3 as L increases, and is not related with ξ_∞ .⁴⁹ One would have to replace ψ by $\psi - \langle \psi \rangle$ in Eq. (7) in order to relate ξ_L to ξ_∞ in the thermodynamic limit. Following current usage, we shall nevertheless refer to ξ_L as “the correlation length”.

Note that, in contrast with $p(q)$ and its first moments, ξ_L takes into account spatial variations of the overlap q .

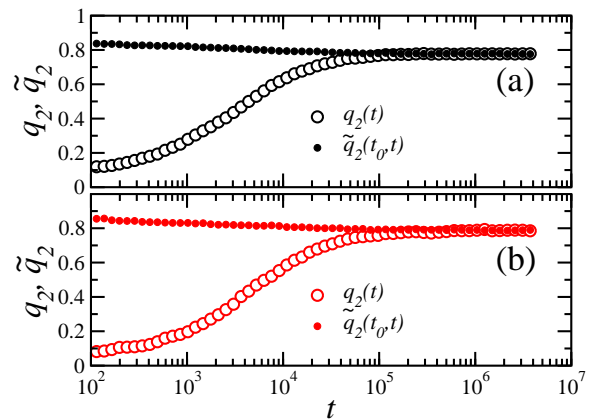


FIG. 1. (Color online) (a) Semilog plots of $\tilde{q}_2(t_0, t)$ (\circ) and $q_2(t)$ (\bullet) vs. time t (measured in Metropolis sweeps) for SC packings of 512 dipoles evolving at $T = 0.2$, the lowest temperature of our TMC simulations. Here, $t_0 = 8 \times 10^6$ Metropolis sweeps. Data points at time t stand for an average over the time interval $[t, 1.2t]$, and over 10^3 samples. (b) The same for RCP.

D. Equilibration Times

It is important to make sure that thermal equilibrium is reached before we start taking measures. To do that, we followed the same procedure as in Ref. 29, by defining, for two replicas of a single sample, the overlap q_t at time t and the average $q_2(t)$ of its square over all samples. Equilibrium is reached when $q_2(t)$ attains a plateau. In order to confirm this result, a second overlap $\tilde{q}_{t_0, t}$

$$\tilde{q}_{t_0, t} \equiv N^{-1} \sum_j \sigma_j(t_0) \sigma_j(t_0 + t), \quad (9)$$

between spin configurations of a single replica taken at times t_0 and $t_0 + t$ is measured as a function of t . Equilibrium imposes that the corresponding average $\tilde{q}_2(t_0, t)$ remains stuck to the above plateau as t varies.²⁹

Plots of $\tilde{q}_2(t_0, t)$ and $q_2(t)$ vs. t are shown in Fig. 1(a) (Fig. 1(b)) for RAD systems on SC lattices (RCP) for $t_0 = 5 \times 10^6$ Metropolis sweeps with $N = 512$ and $T = 0.2$, the lowest value of T in the series of TMC simulations. We have chosen sufficiently large values of t_0 to make sure that $\tilde{q}_2(t_0, t) \approx q_2(t)$ for $t \gtrsim t_0$.

After letting the system equilibrate for a time t_0 , we have taken averages over the time interval $[t_0, 2t_0]$. The values of t_0 and N_s employed in our runs are given in Tables I and II.

It has been shown that equilibration times of individual samples are directly correlated with the roughness of their free-energy landscape.⁵¹ Numerous spikes in the overlap distributions $p_{\mathcal{J}}$ are associated to samples that have several pure states.⁵² The symmetry of the plots of overlap distributions like the ones shown in Fig. 5(a) for SC are an additional check that all the samples are well equilibrated.

III. RESULTS

A. The SG Phase

In this section, we report numerical results for q_2 and ξ_L/L .

A log-log plot of q_2 vs. N for different values of T is shown in Fig. 2 for RAD systems in SC lattices and RCP arrangements. For both models q_2 decreases as N increases, and this occurs at all temperatures. For $T < 0.8$ and the system sizes studied, data points in this figure are consistent with an algebraic decay $q_2 \sim N^{-(1+\eta)}$, following the usual definition of exponent η .⁵³ Plots of q_1 vs. N (not shown) exhibit the same qualitative behavior. All of this is in accordance with quasi-long-range order. Previous simulations³⁴ for the SC were not able to discriminate between the scenario where q_2 tends to a constant value as N grows and the algebraic steady decay shown in Fig. 2. We will return to this point below. From the plots for SC systems, one could extract η for various values of T . The relation $\eta = -1 + a T^2$ fits the data well with $a = 0.45$. Our results disagree with a RSB scenario,³³ in which q_2 does not vanish as $L \rightarrow \infty$.⁵⁴ For even higher temperatures than those shown in Fig. 2, q_2 vs. N curves bend downwards, as expected for the paramagnetic phase. Approximate values of T_{sg} can thus be obtained from such plots, but more accurate methods are given below.

We next examine how ξ_L/L behaves for RAD systems in dense packings with SC and RCP. This has already been done for diluted systems of parallel Ising dipoles.^{27,28} We aim at exploring the behavior of ξ_L/L not only near T_{sg} , but also deep into the SG phase. Recall

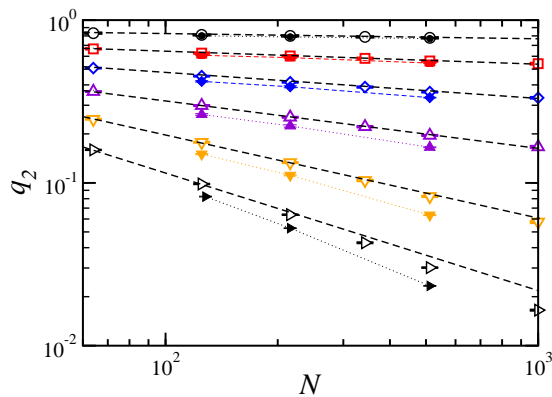


FIG. 2. (Color online) Log-log plots of q_2 vs. the number of dipoles N for SC and RCP. $\circ, \square, \diamond, \triangle, \nabla,$ and \triangleright stand for SC systems at temperatures $T = 0.2, 0.4, 0.6, 0.8, 1.0,$ and 1.2 respectively. $\bullet, \blacksquare, \blacklozenge, \blacktriangle, \blacktriangledown,$ and \blacktriangleright stand for RCP systems at the same temperatures. Dotted lines are guides to the eye. Data sets for larger temperatures deviate from a linear trend (represented by the straight dashed lines), implying a decay faster than a power of $1/N$. Data for the lower temperatures are well fitted by the straight lines.

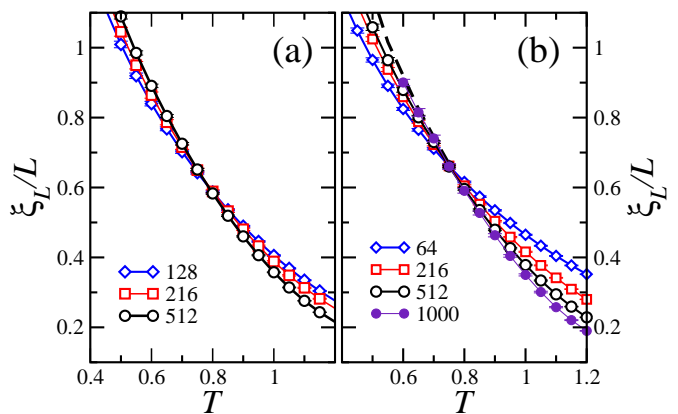


FIG. 3. (Color online) (a) Plots of ξ_L/L vs. T for RCP systems with the number of dipoles N indicated in the figure. Recall that dipoles are placed on a cube of volume $L^3 = N\pi/6\phi$, where ϕ is the volume fraction occupied by the spheres. Continuous lines are guides to the eye. (b) Same as in (a) but for SC systems. Now, $L = N^{1/3}$. The thick dashed line follows from the $1/L \rightarrow 0$ linear extrapolations in the plots of Fig. 4 for $T < T_{sg}$.

that ξ_L becomes a true correlation length in the paramagnetic phase when $\xi_L/L \ll 1$. Then, ξ_L/L falls off as $1/L$ in this phase. On the contrary, ξ_L/L increases with L in the SG phase. The system passes from one phase to the other at a temperature T_{sg} , so that we can reasonably expect that curves of ξ_L/L vs. T for different values of N cross at T_{sg} . All that enables us to extract T_{sg} from those plots. At $T = T_{sg}$, ξ_L/L must become size independent, as expected for a scale free quantity.

Plots of ξ_L/L vs. T are shown in Fig. 3 for different values of N on SC (Fig. 3(a)) and RCP (Fig. 3(b)) arrays. All curves spread out above and below a quite precise crossing point T_{sg} and this fact allows to obtain a precise determination of T_{sg} from the intersection of ξ_L/L vs. T curves as is sometimes done for the EA⁴⁸⁻⁵⁰ and dipolar SG^{27,28} models. For our SC (RCP) systems, curves cross at $T_{sg} = 0.75(2)$ ($T_{sg} = 0.78(3)$).

We now focus on the data for ξ_L at low temperatures, and check if they are consistent with the algebraic decay of $\langle q^2 \rangle$ exhibited in Fig. 2.

In the droplet model picture, in the SG phase $q_2 \neq 0$ and $\langle \psi_0 \psi_r \rangle - \langle \psi_0 \rangle \langle \psi_r \rangle$ is short ranged.³² It then follows that²⁸ $\xi_L^2/L^2 \sim L^3$. No feature exists in the plots of ξ_L/L vs. $1/L$ shown in Fig. 4 suggesting that trend, and this is valid at all temperatures.

Let us assume now that the connected correlation function $\langle \psi_0 \psi_r \rangle - \langle \psi_0 \rangle \langle \psi_r \rangle$ decays as $G(r) \sim 1/r^{(1+\eta)}$ as $r \rightarrow \infty$ while having $q_2 \neq 0$. This behavior fits in with the RSB picture.³³ Then, it follows from Eq. (7) that $\xi_L^2/L^2 \sim L^{1+\eta}$.²⁸ Neither evidence for $\xi_L^2/L^2 \sim L^{1+\eta}$ does appear in Fig. 4. Note that the values of ξ_L/L diminish as a function of $1/L$ for $T < T_{sg}$ and the downward trend becomes steeper as T decreases. On the other hand, from Fig. 2 we know that $|1 + \eta|$ decreases

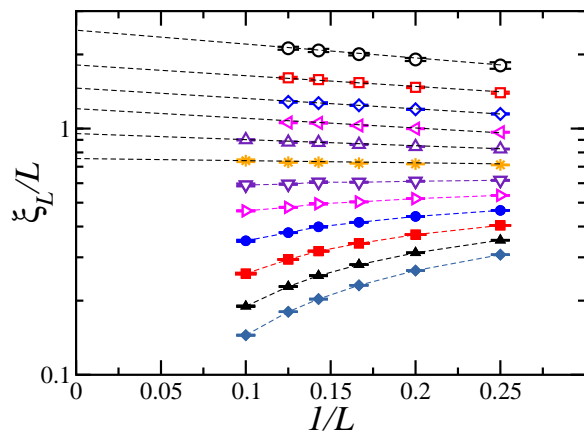


FIG. 4. (Color online) Semilog plots of ξ_L/L vs. $1/L$ for SC systems, and $T = 0.2$ (\circ), $T = 0.3$ (\square), $T = 0.4$ (\diamond), $T = 0.5$ (\triangleleft), $T = 0.6$ (\triangle), $T = 0.7$ ($*$), $T = 0.8$ (∇), $T = 0.9$ (\triangleright), $T = 1.0$ (\bullet), $T = 1.1$ (\blacksquare), $T = 1.2$ (\blacktriangle), and $T = 1.3$ (\blacklozenge). Dashed lines are guides to the eye.

with T . This would lead to ξ_L/L vs. $1/L$ curves which do not become steeper as T decreases, which is in clear contradiction with plots in Fig. 4.

Finally, let us consider $q_2 = 0$ and $\langle \psi_0 \psi_r \rangle = G(r)$ as in the 2D XY model.³¹ It then follows that ξ_L/L becomes independent of L for large L . This is the outcome from $1/L \rightarrow 0$ extrapolations of the dashed straight lines shown in Fig. 4 for $T \lesssim T_{sg}$. Thus, a straightforward interpretation of the data shown in Fig. 4 is that the SG phase for our densely packed RAD systems behaves marginally.⁵⁵

B. Overlap Distributions

It is interesting to study the SG behavior of individual samples. In Fig. 5(a) we plot $p_{\mathcal{J}}(q)$ vs. q for three different samples at temperature $T = 0.2$ for RADs on a SC lattice. Note that $p_{\mathcal{J}}(q)$ distributions are markedly sample-dependent and exhibit several sharp spikes centered well away from $q \approx \pm 1$. Similar behavior has been found for the EA and SK models.^{52,56} The positions and heights of the spikes in the region $q \in (-Q, Q)$ for, say, $Q \approx 1/2$ change greatly from sample to sample. These inner peaks arise from cross overlaps between different pure states. We name these spikes *cross-overlap* (CO) spikes. Their number in $p_{\mathcal{J}}(q)$ is closely related to the number of pure states.⁵² At higher temperatures (not shown), thermal fluctuations render individual spikes so wide that they overlap and become not clearly discernible. Then, in order to examine CO spikes we were compelled to choose $T_{min} \approx T_{sg}/4$ in our simulations.

Figure 5(b) shows the mean overlap distribution $p(q)$ for SC arrays at $T = 0.2$ for different values of N . $p(q)$ exhibits two large peaks at $\pm q_m$ with $q_m \approx 1$ that correspond to the self overlap of pure states. We find that

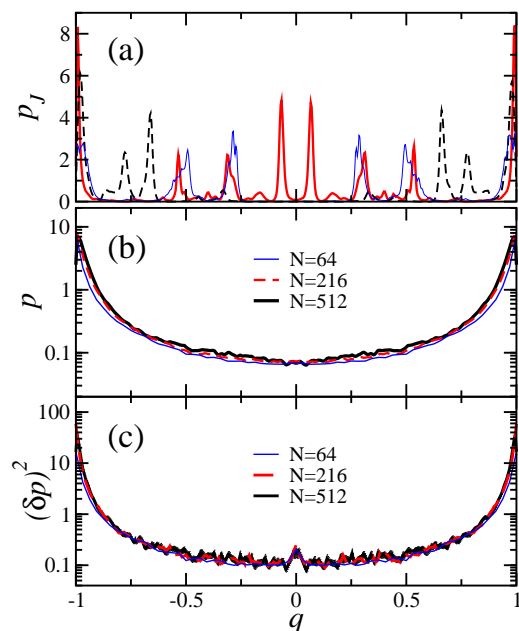


FIG. 5. (Color online) (a) Overlap distributions $p_{\mathcal{J}}(q)$ for SC systems with $N = 512$ and $T = 0.2$ for three samples with different realizations of disorder (b) Plots of the averaged distribution $p(q)$ vs. q for SC systems with $T = 0.2$, and the values of N shown. (c) Same as in (b) for $(\delta p)^2$. Similar results obtain for RCP systems.

$p(q)$ is approximately flat in the region of small values of q , with $p(0) \neq 0$. Note that $p(0)$ is essentially independent of N , as previously found for the SK and EA models.^{36,57} This behavior is in conflict with the droplet picture of SGs, for which $p(0) \sim N^{-\theta}$.³²

Plots of $(\delta p)^2$ vs. q are shown for SC arrays at the same temperature in Fig. 5(c). We obtain (not shown) qualitatively similar plots for RCP systems. $(\delta p)^2$, which is a measure of sample-to-sample fluctuations of $p_{\mathcal{J}}(q)$ from the average $p(q)$, does not change appreciably with N . According to the RSB scenario, $p_{\mathcal{J}}(q)$ should exhibit many CO spikes that become Dirac delta functions as N increases, bringing about a diverging $(\delta p)^2$ in the thermodynamic limit.

In order to improve the accuracy, we consider the integrated probability functions

$$X_{\mathcal{J}}^Q \equiv \int_{-Q}^{+Q} p_{\mathcal{J}}(q) dq, \quad (10)$$

$$\Delta_{\mathcal{J}}^Q \equiv \left(\int_{-Q}^{+Q} \{p_{\mathcal{J}}(q) - p(q)\}^2 dq \right)^{1/2}, \quad (11)$$

and compute their related sample averages X^Q and Δ^Q .

Plots of X^Q vs. T are shown for $Q = 1/2$ in Figs. 6(a), 6(b), and 6(c) for SC, RCP systems and the SK model respectively. In all cases, X^Q appears to be size independent at temperatures well below T_{sg} , in agreement

with mean field predictions for the SK model. This is in clear contrast to the droplet picture, for which X^Q is predicted to vanish as $N^{-\Theta}$.³² Finally, we note that in all cases $X^Q \propto T$ at low temperatures.

Plots of Δ^Q vs. T for RADs in Figs. 7(a) and 7(b) for SC and RCP suggest that Δ^Q does not diverge as N increases at very low temperatures. In marked contrast, the corresponding plots for the SK model exhibited in Fig. 7(c) show that Δ^Q clearly increases with N at all temperatures below T_{sg} , in agreement with the RSB scenario.

C. Cross Overlap Spikes

The shape and width of CO spikes from a *pair correlation function* was studied in previous work.⁵⁸ With $f_{\mathcal{J}}(q_1, q_2) \equiv p_{\mathcal{J}}(q_1)p_{\mathcal{J}}(q_2)$, we define

$$G_{\mathcal{J}}^Q(q) \equiv \int_0^Q \int_0^Q dq_1 dq_2 \delta(q_2 - q_1 - q) f_{\mathcal{J}}(q_1, q_2), \quad (12)$$

and $G^Q(q)$ as the average of $G_{\mathcal{J}}^Q(q)$ over samples. We have computed the normalized function

$$g^Q(q) \equiv \frac{G^Q(q)}{\int_{-Q}^{+Q} G^Q(q) dq}, \quad (13)$$

which is the conditional probability density that $q = q_2 - q_1$, given that $q_1, q_2 \in (0, Q)$.

At very low temperatures, $g^Q(q)$ could be interpreted as the averaged shape of all CO spikes provided that individual spikes in $p_{\mathcal{J}}(q)$ distributions do not overlap each other.²⁹ Temperatures as low as $T_{sg}/4$ are needed to observe this regime (see Fig. 5(a)). Plots of g^Q vs. q for $Q = 1/2$ and $T = 0.2$ are shown in Figs. 8(a) and 8(b) for RADs on SC and RCP arrays respectively, and in Fig. 8(c) for the SK model at $T = 0.24$. g^Q curves appear to be very pointed and narrow in all cases.

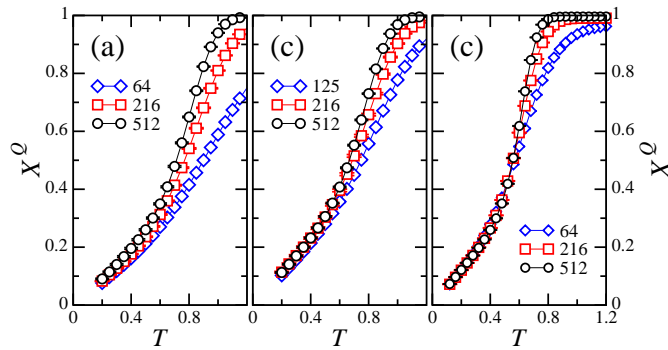


FIG. 6. (Color online) (a) Plots of X^Q vs. T for SC systems, $Q = 1/2$ and the values of N indicated in the figure. (b) The same plots for RCP systems. (c) The same plots for the SK model.

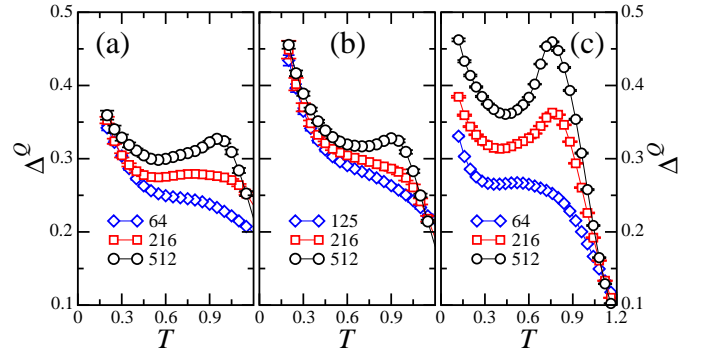


FIG. 7. (Color online) (a) Plots of Δ_Q vs. T for SC systems, with $Q = 1/2$ and the values of N indicated in the figure. (b) The same plots for RCP systems. (c) The same plots for the SK model.

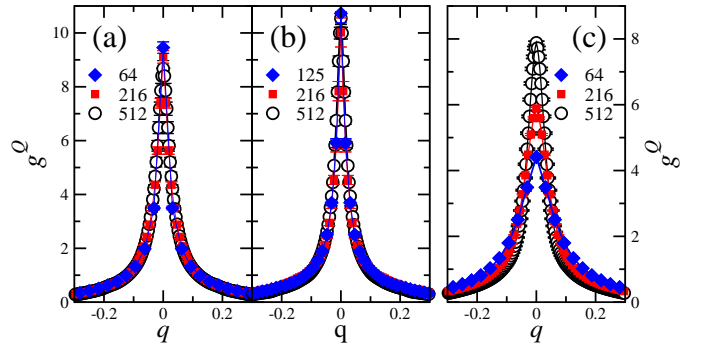


FIG. 8. (Color online): (a) Plots of g^Q vs. q for SC systems at $T = 0.2$, with $Q = 1/2$ and the values of N indicated in the figure. (b) The same plots for RCP systems. (c) The same plots for the SK model at $T = 0.24$. Note that $T \approx T_{sg}/4$ in all three cases.

Note that curves for RAD systems in Figs. 8(a) and 8(b) do not change appreciably with system size for both SC and RCP arrangements. In contrast, g^Q curves for SK in Fig. 8(c) become sharper as N increases. This is as expected for the mean-field RSB scenario, in which CO spikes become Dirac delta functions in the macroscopic limit.

Given that $g^Q(q)$ is a normalized distribution, we compute its width as $w^Q \equiv 1/g^Q(0)$.⁵⁸ Plots of w^Q vs. T are shown in Figs. 9(a) and 9(b) for RADs on SC and RCP arrays respectively. In both cases, w^Q does not change appreciably with system size, suggesting that the width of CO spikes do not vanish in the $N \rightarrow \infty$ limit for all temperatures below T_{sg} . On the other hand, plots of w^Q vs. T for the SK model displayed in Fig. 9(c) indicate a vanishing width (curves actually go like $w^Q \sim N^{-3/2}$),²⁹ in agreement with the RSB picture.

D. Cumulative Distributions

Pair correlation functions do not provide information about the height of CO spikes in the $(-Q, Q)$ region. Yucesoy *et al.*⁵⁶ have proposed an observable that depends on the height of CO spikes in SG models. They consider the maximum value of $p_{\mathcal{J}}(q)$ for $q \in (-Q, Q)$,

$$\tilde{p}_{\mathcal{J}}^Q \equiv \max\{p_{\mathcal{J}}^Q(q) : |q| < Q\}, \quad (14)$$

and count a sample as *peaked* if $\tilde{p}_{\mathcal{J}}^Q$ exceeds some specified value z . Then, the cumulative distribution $\Pi_c^{\tilde{p}}(z)$ of *non-peaked* samples is computed as a function of z . Plots of $\Pi_c^{\tilde{p}}$ vs. z for RAD on RCP arrays are shown in Fig. 10(a) for $T = 0.2$ and $Q = 1/2$. They suggest that $\Pi_c^{\tilde{p}}$ becomes size-independent for $N \geq 216$. In contrast, simulations for the SK model have shown that $\Pi_c^{\tilde{p}}(z)$ clearly decreases as N increases for $z \gtrsim 0.5$ at low temperatures.²⁹ The latter is in agreement with the RSB picture, for which CO spikes become Dirac delta functions in the $N \rightarrow \infty$ limit.

Given that $X_{\mathcal{J}}^Q$ is a (\mathcal{J} -dependent) random variable, it is interesting to explore how this variable is distributed. Following Ref. 59, we define its cumulative distribution $\Pi_c^X(z)$ as the fraction of samples having $X_{\mathcal{J}}^Q < z$. Semilog plots of Π_c^X vs. z for RAD on RCP arrays displayed in Fig. 10(b) appear to be size independent and exhibit a power-law behavior of $\Pi_c^X(z)$ for small z . Our results for Π_c^X are not in contradiction with a RSB scenario.

IV. CONCLUSIONS AND DISCUSSION

We have studied ensembles of dense packings of identical classical Ising dipoles at low temperature. Each dipole is the total magnetic moment of a single-domain spherical NP (due to their smallness, NP admit one single domain). We assume that the local anisotropies of the NP oblige the magnetic moment to lie along an easy

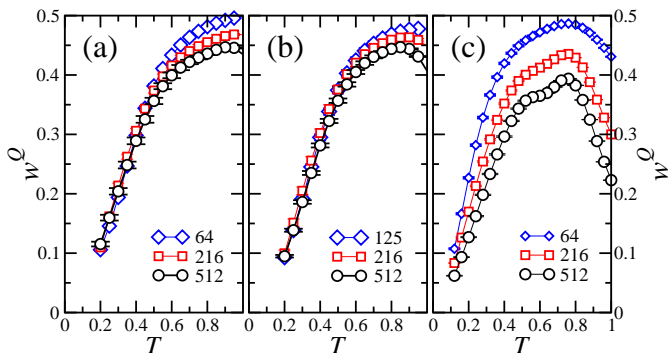


FIG. 9. (Color online) (a) Plots of w^Q vs. q for SC systems for $Q = 1/2$ and the values of N indicated in the figure. (b) The same plots for RCP systems. (c) The same plots for the SK model.

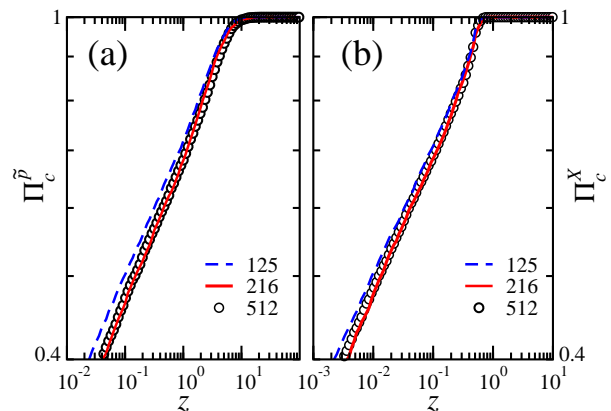


FIG. 10. (Color online) (a) Plots of the cumulative distribution $\Pi_c^{\tilde{p}}$ vs. z for RCP systems, with $Q = 1/2$, $T = 0.2$ and the values of N indicated in the figure. (b) Same as in (a) for the cumulative distribution Π_c^X .

axis. The arbitrary orientation of all NP provokes that each dipole is randomly oriented.

We consider random axis dipole (RAD) systems with two types of packings: (i) the NP are placed on SC lattices and (ii) random closed packings (RCP) that fill a volume fraction $\phi_0 = 0.64$, as in recent experiments with maghemite NP.

We have focused on the role played by the dipolar interaction in the thermodynamical equilibrium. Dipoles were allowed to flip between up and down directions along one of their easy axes, regardless of the height of the anisotropy barriers.

Previous simulations for RADs on SC lattices provided evidence for the existence of a transition from paramagnetic to SG phases. However, numerical results did not lead to any firm conclusion on the nature of this SG phase. From the study of the overlap parameter q and their associated correlation length, we have found a marginal behavior for RADs on SC and RCP lattices for temperatures below a temperature T_{sg} . Actually, the similarities between SC and RCP systems extend to all observables we have explored.

From the variation of ξ_L with T and L we have found $T_{sg} = 0.75(2)$ and $T_{sg} = 0.78(3)$ for SC and RCP lattices respectively. In the SG phase we have observed (i) an algebraic decay of q_2 with the system size, and (ii) absence of any divergence in the values of the ratio ξ_L/L as the system size increased (see section III.A). This marginal behavior fits neither the droplet model nor a RSB scenario.

In spite of the existence of *quasi-long-range* SG order, the overlap distributions $p_{\mathcal{J}}(q)$ are comb-like and markedly sample dependent, like it occurs for the EA and the SK models.^{52,56,58} We have studied the sample-to-sample statistics of $p_{\mathcal{J}}(q)$ for $q \in (-Q, Q)$ at low temperatures (section III.B), finding that $p(q)$ and $\delta p(q)^2$ (as well as X^Q and Δ^Q) do not vary with N . By computing also the averaged width w^Q of the spikes found in

$p_{\mathcal{J}}(q)$ distributions (section III.C), we conclude that w^Q does not vanish in the thermodynamic limit. Accordingly, the fraction of samples with spikes higher than a certain threshold does not change with N at low temperatures (section III.D).

Altogether, these results are in agreement with the above-mentioned marginal behavior. Our MC data for the SK model illustrate that there is some conflict between RSB predictions and our results for RAD. It is worth mentioning that our findings for densely packed RAD systems resemble the behavior of RAD systems with strong dilution³⁰ and that of systems of parallel

Ising dipoles in site-diluted lattices^{28,29}.

ACKNOWLEDGEMENTS

We thank the Centro de Supercomputación y Bioinformática at University of Málaga, and to Institute Carlos I at University of Granada for their generous allocations of computer time in clusters Picasso, and Proteus. J.J.A. thanks for financial support from the Ministerio de Economía y Competitividad of Spain, through Grant No. FIS2013-43201-P. We are grateful to J. F. Fernández for helpful discussions.

-
- * e-mail address: jjalonso@uma.es
† E-mail address: alles@pi.infn.it
- ¹ D. Fiorani, and D. Peddis, *J. Phys.: Conference Series* **521**, 012006 (2014).
 - ² R. P. Cowburn, *Philos. Trans. R. Soc. London, Ser. A* **358**, 281 (2000); R. J. Hicken, *ibid.* **361**, 2827 (2003).
 - ³ R. F. Wang, C. Nisoli, R. S. Freitas, J. Li, W. McConville, B. J. Cooley, M. S. Lund, N. Samarth, C. Leighton, V. H. Crespi and P. Schiffer, *Nature (London)* **439**, 303 (2006).
 - ⁴ S. Bedanta, and W. Kleeman *J. Phys. D: Appl. Phys.* **42** 013001 (2009); S. A. Majetich and M. Sachan, *J. Phys. D: Appl. Phys.* **39**, R407 (2006).
 - ⁵ N. A. Frey, S. Peng, K. Cheng, and S. Sun, *Chem. Soc. Rev.* **38**, 2532 (2009).
 - ⁶ S. D. Bader *Rev. Mod. Phys.* **78**, 1 (2006).
 - ⁷ L. Néel, *Géophysique* **5**, 99 (1949); P. Allia, M. Coisson, P. Tiberto, F. Vinai, M. Knobel, M. A. Novak, and W. C. Nunes *Phys. Rev. B* **64**, 144420 (2001).
 - ⁸ M. Mézard, G. Parisi, and M. Virasoro, *Spin Glass Theory and Beyond* (World Scientific, Singapore, 2004).
 - ⁹ J. Luttinger and L. Tisza, *Phys. Rev.* **72**, 257 (1947); J. F. Fernández and J. J. Alonso, *Phys. Rev. B* **62**, 53 (2000).
 - ¹⁰ O. Kasuyutich, R. D. Desautels, B. W. Southern, and J. van Lierop *Phys. Rev. Lett.*, **104**, 127205 (2010).
 - ¹¹ Y. Takagaki, C. Herrmann and E. Wiebicke, *J. Phys.: Condens. Matter* **20**, 225007 (2008).
 - ¹² S. Nakamae, C. Crauste-Thibierge, D. L'Hôte, E. Vincent, E. Dubois, V. Dupuis, and R. Perzynski, *Appl. Phys. Lett.*, **101**, 242409 (2010); S. Nakamae, *J. Magn. Magn. Mater.* **355** (2014).
 - ¹³ S. Sahoo, O. Petravic, W. Kleemann, P. Nordblad, and P. Svedlindh, *Phys. Rev. B* **67**, 214422 (2003).
 - ¹⁴ S. Mørup *Europhys. Lett.* **28**, 671 (1994).
 - ¹⁵ D. L. Stein and C. M. Newman, *Spin Glasses and Complexity* (Princeton University Press, Princeton, NJ, 2012).
 - ¹⁶ W. Luo, S. R. Nagel, T. F. Rosenbaum, and R. E. Rosensweig, *Phys. Rev. Lett.* **67**, 2721 (1991); T. Jonsson, J. Mattsson, C. Djurberg, F. A. Khan, P. Nordblad and P. Svedlindh, *Phys. Rev. Lett.* **75**, 4138 (1995); G. G. Kenning, G. F. Rodriguez and R. Orbach, *Phys. Rev. Lett.* **97**, 057201 (2006).
 - ¹⁷ K. Binder and A. P. Young, *Rev. Mod. Phys.* **58**, 801 (1986).
 - ¹⁸ J. O. Andersson, C. Djurberg, T. Jonsson, P. Svedlindh, and P. Nordblad, *Phys. Rev. B* **56**, 13983 (1997).
 - ¹⁹ J. García-Otero, M. Porto, J. Rivas and A. Bunde, *Phys. Rev. Lett.* **84**, 167 (2000); M. Ulrich, J. García-Otero, J. Rivas, and A. Bunde, *Phys. Rev. B* **67**, 024416 (2003).
 - ²⁰ O. Iglesias and A. Labarta, *Phys. Rev. B* **70**, 144401 (2004).
 - ²¹ Y. Sun, M. B. Salamon, K. Garnier, and R. S. Averback, *Phys. Rev. Lett.* **91**, 167206 (2003).
 - ²² V. Russier, C. de-Montferrand, Y. Lalatonne, and L. Motte *J. Appl. Phys.* **114**, 143904 (2013); V. Russier *J. Magn. Magn. Mater.* **409**, 50 (2016).
 - ²³ M. Woińska, J. Szczytko, A. Majhofer, J. Gosk, K. Dziatkowski, and A. Twardowski *Phys. Rev. B* **88**, 144421 (2013).
 - ²⁴ S. Russ, and A. Bunde, *Phys. Rev. B* **75**, 174445 (2007).
 - ²⁵ J. A. De Toro, S. S. Lee, D. Salazar, J. L. Cheong, P. S. Normile, P. Muñiz, J. M. Riveiro, M. Hillenkamp, F. Tournus, A. Amion, and P. Nordblad *Appl. Phys. Lett.* **102**, 183104 (2013).
 - ²⁶ M. S. Andersson, R. Mathieu, S. S. Lee, P. S. Normile, G. Singh, P. Nordblad, and J. A. De Toro *Nanotechnology* **26** 475703 (2015).
 - ²⁷ K. M. Tam, and M. J. P. Gingras, *Phys. Rev. Lett.* **103**, 087202 (2009); J. C. Andresen, H. G. Katzgraber, V. Oganesyan, and M. Schechter, *Phys. Rev. X* **4**, 041016 (2014).
 - ²⁸ J. J. Alonso and J. F. Fernández, *Phys. Rev. B* **81**, 064408 (2010).
 - ²⁹ J. J. Alonso, *Phys. Rev. B* **91**, 094406 (2015).
 - ³⁰ J. F. Fernández and J. J. Alonso, *Phys. Rev. B* **79**, 214424 (2009).
 - ³¹ J. M. Kosterlitz and D. J. Thouless, *J. Phys. C* **6**, 1181 (1973); J. M. Kosterlitz, *ibid.* **7**, 1046 (1974); J. F. Fernández, M. F. Ferreira, and J. Stankiewicz, *Phys. Rev. B* **34**, 292-300 (1986); H. G. Evertz and D. P. Landau, *Phys. Rev. B* **54**, 12302 (1996).
 - ³² D. S. Fisher and D. A. Huse, *J. Phys. A* **20**, L1005 (1987); D. S. Fisher and D. A. Huse, *Phys. Rev. B* **38**, 386 (1988).
 - ³³ G. Parisi, *Phys. Rev. Lett.* **43**, 1754 (1979); *ibid* **50**, 1946 (1983).
 - ³⁴ J. F. Fernández, *Phys. Rev. B* **78**, 064404 (2008).
 - ³⁵ D. Sherrington and S. Kirkpatrick, *Phys. Rev. Lett.* **35**, 1792 (1975); S. Kirkpatrick and D. Sherrington, *Phys. Rev. B* **17**, 4384 (1978).
 - ³⁶ D. J. Thouless, P. W. Anderson, and R. G. Palmer, *Philos. Mag.* **35**, 593 (1977); A. J. Bray and M. A. Moore, *Phys.*

- Rev. Lett.* **41**, 1068 (1978).
- ³⁷ H. G. Katzgraber, M. Palassini, and A. P. Young, *Phys. Rev. B* **63**, 184422 (2001).
- ³⁸ S. F. Edwards and P. W. Anderson, *J. Phys. F*, **5**, 965 (1975).
- ³⁹ R. N. Bhatt and A. P. Young, *Phys. Rev. Lett.* **54**, 924 (1985); R. N. Bhatt and A. P. Young, *Phys. Rev. B* **37**, 5606 (1988).
- ⁴⁰ B. D. Lubachevsky, and F. H. Stillinger, *J. Stat. Phys.* **60**, 561 (1990).
- ⁴¹ M. Skoge, A. Donev, F.H. Stillinger, and S. Torquato, *Phys. Rev. E* **74**, 041127 (2006).
- ⁴² S. Torquato, and F. H. Stillinger, *Rev. Mod. Phys.* **82**, 2633 (2010).
- ⁴³ P. Ewald, *Ann. Phys. (Leipzig)* **64**, 253, (1921)
- ⁴⁴ M. P. Allen and D. J. Tildesley, *Computer simulation of Liquids*, 1st ed. (Clarendon, Oxford, 1987).
- ⁴⁵ Z. Wang, and C. Holm, *J. of Chem. Phys.* **115**, 6351 (2001).
- ⁴⁶ E. Marinari and G. Parisi, *Europhys. Lett.* **19**, 451 (1992); K. Hukushima and K. Nemoto, *J. Phys. Soc. Jpn.* **65**, 1604 (1996).
- ⁴⁷ N. A. Metropolis, A. W. Rosenbluth, M. N. Rosenbluth, A. H. Teller, and E. Teller, *J. Chem. Phys.* **21**, 1087 (1953).
- ⁴⁸ M. Palassini and S. Caracciolo, *Phys. Rev. Lett.* **82**, 5128 (1999).
- ⁴⁹ H. G. Ballesteros, A. Cruz, L. A. Fernandez, V. Martín-Mayor, J. Pech, J. J. Ruiz-Lorenzo, A. Tarancón, P. Téllez, C. L. Ullod, and C. Ungil *Phys. Rev. B* **62**, 14237 (2000).
- ⁵⁰ H. G. Katzgraber, M. Körner, and A. P. Young, *Phys. Rev. B* **73**, 224432 (2006).
- ⁵¹ B. Yucesoy, J. Machta and H. G. Katzgraber, *Phys. Rev. E* **87**, 012104 (2013).
- ⁵² T. Aspelmeier, A. Billoire, E. Marinari, and M. A. Moore, *J. Phys. A* **41**, 324008 (2008).
- ⁵³ M. E. Fisher, *Rev. Mod. Phys.* **70**, 653 (1998).
- ⁵⁴ One could argue, however, that larger values of N are needed to discard a scenario with a non-vanishing q_2 and a diverging correlation length.
- ⁵⁵ This might seem to be in contradiction to the fact that ξ_L/L curves do clearly cross, as shown in Figs. 3(a) and 3(b), and that, as pointed out in Ref. 49, ξ_L/L vs. T curves merge, not cross, for the 2D XY model, as $T \rightarrow T_{sg}$ from above. Some specific examples in Ref. 28 illustrate how both merging and spreading as T decreases below T_{sg} can occur depending on some minor details of $G(r)$.
- ⁵⁶ B. Yucesoy, H. G. Katzgraber, and J. Machta, *Phys. Rev. Lett.* **109**, 177204 (2012).
- ⁵⁷ H. G. Katzgraber, M. Palassini, and A. P. Young, *Phys. Rev. B* **63**, 184422 (2001).
- ⁵⁸ J. F. Fernández and J. J. Alonso, *Phys. Rev. B* **86**, 140402(R) (2012); J. F. Fernández and J. J. Alonso, *Phys. Rev. B* **87**, 134205 (2013).
- ⁵⁹ A. Billoire, A. Maiorano, E. Marinari, V. Martin-Mayor, and D. Yllanes, *Phys. Rev. B* **90**, 094201 (2014).